Evidence for a Novel Bursting Mechanism in Rodent Trigeminal Neurons

Christopher A. Del Negro,* Chie-Fang Hsiao,* Scott H. Chandler,* and Alan Garfinkel*#
*Department of Physiological Science and #Department of Medicine (Cardiology), University of California at Los Angeles,
Los Angeles, California 90095-1568 USA

ABSTRACT   We investigated bursting behavior in rodent trigeminal neurons. The essential mechanisms operating in the biological systems were determined based on testable predictions of mathematical models. Bursting activity in trigeminal motoneurons is consistent with a traditional mechanism employing a region of negative slope resistance in the steady-state current-voltage relationship (Smith, T. G. 1975. *Nature.* 253:450–452). However, the bursting dynamics of trigeminal interneurons is inconsistent with the traditional mechanisms, and is far more effectively explained by a new model of bursting that exploits the unique stability properties associated with spike threshold (Baer, S. M., T. Erneux, and J. Rinzel. 1989. *SIAM J. Appl. Math.* 49:55–71).

INTRODUCTION

Neuronal bursting is produced as slow membrane processes dynamically modulate the activity of faster membrane processes responsible for action potentials. Specific mechanisms for bursting have been studied mathematically and can be differentiated based on mechanism and phenomenology (Bertram et al., 1995).

Traditional bursting systems require inactivation-resistant inward currents that create a region of negative slope resistance (NSR) in the steady-state (or quasi-steady-state) current-voltage (*I-V*) relationship (Canavier et al., 1991; Li et al., 1996; Schwindt and Crill, 1980; Smith, 1975). The N-shaped *I-V* relationship provides the potential for two stable voltage states, one on each side of spike threshold (one state is quiescent and the other oscillatory). The cell then alternates between the two states during bursting (although it need not be bistable). The regenerative region of inward current separating the stable states predicts phenomenological features that can be used to identify traditional bursting in the laboratory, where membrane potential is frequently the only measurable variable: 1) cells can be locked into quiescent or active states by sufficient current bias; 2) bursts initiate rapidly, in contrast to the slow trajectory of the quiescent phase, with a marked upswing in membrane potential; 3) spikes in the active phase emerge at full amplitude from the steady-state membrane potential of the quiescent phase; and 4) burst termination is accompanied by a decline in spike frequency. Traditional bursting has been observed in many experimental preparations. Canonical examples include the pancreatic β cell (Ashcroft and Rorsman, 1989; Atwater et al., 1980) for bistable (or type 1; Bertram et al., 1995) bursting and *Aplysia*'s R15 neuron for parabolic (or type 2; Bertram et al., 1995) burst-

ing (Benson and Adams, 1989; Canavier et al., 1991; Rinzel and Lee, 1987).

Another mechanism for bursting has been proposed theoretically (Av-Ron et al., 1993; Bertram et al., 1995; Honerkamp et al., 1985; Rinzel, 1987, Fig. 4; Wang, 1993b) but has not yet been identified experimentally. This novel mechanism, which we will call type 3 bursting, based on Bertram's classification scheme (Bertram et al., 1995), does not require a region of NSR in the steady-state *I-V* relationship, but rather exploits unique stability properties near spike threshold. The mechanistic framework also predicts phenomenology that can be used empirically to identify type 3 bursting: 1) bursting evolves from intermittent discharge as cells are depolarized by current bias, 2) bursts initiate with a slow linear voltage trajectory (as opposed to a rapid voltage upswing in traditional bursting), 3) full-amplitude spikes emerge from subthreshold oscillations (as opposed to a steady-state potential as in traditional bursting), and 4) spike frequency may not decline at burst termination.

Bursting mechanisms in rodent trigeminal neurons controlling jaw movements can be assigned based on the theoretical predictions above. Using experimental data, we identify, for the first time, type 3 bursting dynamics in a biological system: the neonatal rat trigeminal interneuron (TI). We contrast this new mechanism with the traditional bursting that occurs in trigeminal motoneurons (TMNs) (Hsiao et al., 1998).

MATERIALS AND METHODS

Electrophysiological experiments were performed on TIs obtained from 300-μm-thick transverse slices of neonatal rat brain stem (0–7 days). Slices were perfused (4 ml/min) at room temperature by oxygenated solution containing (in mM) 124 NaCl, 3 KCl, 1.25 NaH$_2$PO$_4$, 26 NaHCO$_3$, 10 D-glucose, 2 CaCl$_2$, and 2 MgCl$_2$. Whole-cell patch-clamp recordings were made with an Axopatch-1D amplifier (Axon Instruments, Burlingame, CA). Patch electrodes (3–7 MΩ) were filled with the following solution (in mM): 9 NaCl, 140 KCl, 1 MgCl$_2$, 10 HEPES buffer, 0.2 EGTA, 10 phosphocreatine, 0.1 leupeptin, 5 K$_2$-ATP, and 1 Na$_3$-GTP (pH $\cong$ 7.25).

Intracellular recordings from TMNs were obtained from $450\text{-}\mu\text{m}$-thick transverse brain stem slices from adolescent guinea pigs (150–250 g) as shown previously (Hsiao et al., 1998). Slices were perfused in a gas-interface chamber at 33–34°C with oxygenated solution containing (in mM) 130.0 NaCl, 3.0 KCl, 1.25 KH_2PO_4, 20.0 $NaHCO_3$, 10.0 D-glucose, 2.4 $CaCl_2$, and 1.3 $MgSO_4$. Microelectrodes were filled with 3 M KCl (15–20 $M\Omega$). Experiments were performed with an Axoclamp 2A amplifier (Axon Instruments).

Bursting dynamics were studied in minimal mathematical models by exploiting the disparate time scales of fast and slow membrane processes; these define the FAST and SLOW subsystems of full models (Rinzel, 1987). All models have the same general form:

$$\text{FAST:} \qquad dx/dt = F(x, z), \qquad (1)$$

$$\text{SLOW:} \qquad dz/dt = \alpha G(x, z), \qquad (2)$$

where $x \in \mathbb{R}^2$, $z \in \mathbb{R}^n$, and $0 < \alpha \ll 1$.
The FAST subsystem is a two-dimensional abstraction of action potential dynamics according to Fitzhugh and Hindmarsh-Rose (Fitzhugh, 1961; Hindmarsh and Rose, 1982). This treatment preserves the essential features of spike trajectory and frequency while facilitating the geometric analysis of FAST dynamics in planar state space. The steady-state and oscillatory solutions of FAST were determined by allowing all FAST variables to assume equilibrium values, with the SLOW variables treated as parameters. Formally, with z as a vector of parameters, the steady-state solutions of FAST satisfy

$$0 = F(x_{ss}; z), \qquad (3)$$

where x_{ss} is the equilibrium value for x at given z. Oscillatory solutions of FAST satisfy

$$x_{osc}(t + \tau; z) = x_{osc}(t; z), \qquad (4)$$

where x_{osc} represents the x values and τ represents the period of the limit cycle. A bifurcation diagram of solutions to FAST can be generated using z as a control parameter, where x_{ss} is a continuous collection of stable and unstable critical points and x_{osc} is displayed by the maximum and minimum voltage amplitudes of the limit cycles (x_{max} and x_{min}, respectively). The collection of stable and unstable equilibrium points represents a slow manifold, because the system travels slowly along this structure during bursting cycles when SLOW variables interact dynamically with FAST in the evolving system (e.g., Fig. 1 A). The transitions between quiescent and active phases of bursting occur at bifurcations of FAST. This analysis, pioneered by Rinzel (Rinzel, 1987; Rinzel and Lee, 1986), presumes that in the full model, FAST relaxes to steady-state behavior at every point of SLOW, justifying the bifurcation diagram obtained by treating SLOW as a parameter (which is reasonable if $0 < \alpha \ll 1$). Simulations employed a fourth-order Runge-Kutta, adaptive time-step integration method (maximum accuracy parameter 10^{-3}) (ModelMaker 3.0; Cherwell Scientific, Oxford, UK). Physiological data were analyzed using Datapac III, v. 1.47 (Run Technologies, Irvine, CA).

RESULTS

Mathematical bursting models

Traditional bursting mechanisms utilize a Z-shaped slow manifold whose structure is directly related to and generated by the region of NSR in the steady-state *I-V* relationship. The simplest form of traditional bursting occurs when the SLOW subsystem is one-dimensional ($n = 1$ in Eq. 2) (Fig. 1 A). The quiescent phase of bursting in the Hindmarsh-Rose model (see Appendix) takes place on the lower stable branch of the slow manifold; SLOW causes the evolving system to approach the left knee of the manifold (z is decreasing). The active phase begins when the system rounds the left knee of the slow manifold, where the unstable middle branch (composed of saddle points) and the lower stable branch meet in a saddle-node bifurcation (Hindmarsh and Rose, 1984). At the saddle node, the limit cycle attractor surrounding the upper branch of the slow manifold becomes globally attracting. Therefore, the system begins its oscillatory phase asymptotically close to but outside of this limit cycle. This topology ensures that spikes emerge at full amplitude in the active phase (Fig. 1 *A*).

During the active phase, SLOW sweeps the periodic solution through a hysteresis loop along the upper branch of the slow manifold. Within this loop, stable oscillatory and stable steady-state attractors coexist for given values of z. The periodic solution continues until the spike oscillation contacts the unstable middle branch (Fig. 1 *A*). At this intersection, the stable and unstable manifolds of the saddle point converge with the limit cycle, resulting in a homoclinic orbit (Wang, 1993a). The homoclinic orbit signals burst termination, because changes due to SLOW ultimately cause the system to cross the stable manifold of the saddle (a separatrix) and return to the lower stable branch of the slow manifold, thus beginning the quiescent phase. As mentioned, this type of traditional bursting exhibits hysteresis-based bistability, because the FAST subsystem has two solutions (one quiescent, one oscillatory) at z values encountered during burst cycles (Fig. 1 *A*).

If SLOW is planar ($n = 2$ in Eq. 2), parabolic bursting may result (Bertram et al., 1995; Butera et al., 1996; Rinzel and Lee, 1987). In the Chay-Cook model of parabolic bursting (Appendix), the slow manifold is a Z-shaped surface (Fig. 1 *B*). Active phase initiation similarly occurs via a saddle-node bifurcation at the left knee of the slow manifold, where c values are low and s is increasing. As the active phase ensues, both s and c increase. Therefore, during the active phase, the limit cycle remains along the upper branch of the slow manifold, left of the left knee (Fig. 1 *B*). Although c continues to grow throughout the burst, s consequently declines, and the trajectory again contacts the left knee of the slow manifold (at higher c values). Therefore, the active phase of parabolic bursting terminates via a homoclinic orbit when the spike oscillation contacts the saddle-node singularity. There is no hysteresis-based bistability (as in Fig. 1 *A*) in parabolic bursting models. The bifurcations associated with phase transition are both formed where a saddle-node singularity intersects a limit cycle, called a saddle-node-on-an-invariant-circle (Bertram et al., 1995; Guckenheimer et al., 1997). The unbounded period associated with these homoclinic transitions gives rise to the characteristic parabola seen in the spike frequency-time plot for which parabolic bursting is named (Rinzel and Lee, 1987, see their figure 6). However, the acceleration of spike frequency at burst onset is less obvious in some bursting models (such as that in Fig. 1 *B*), where the first transition (burst initiation) occurs more rapidly than the second (termination).
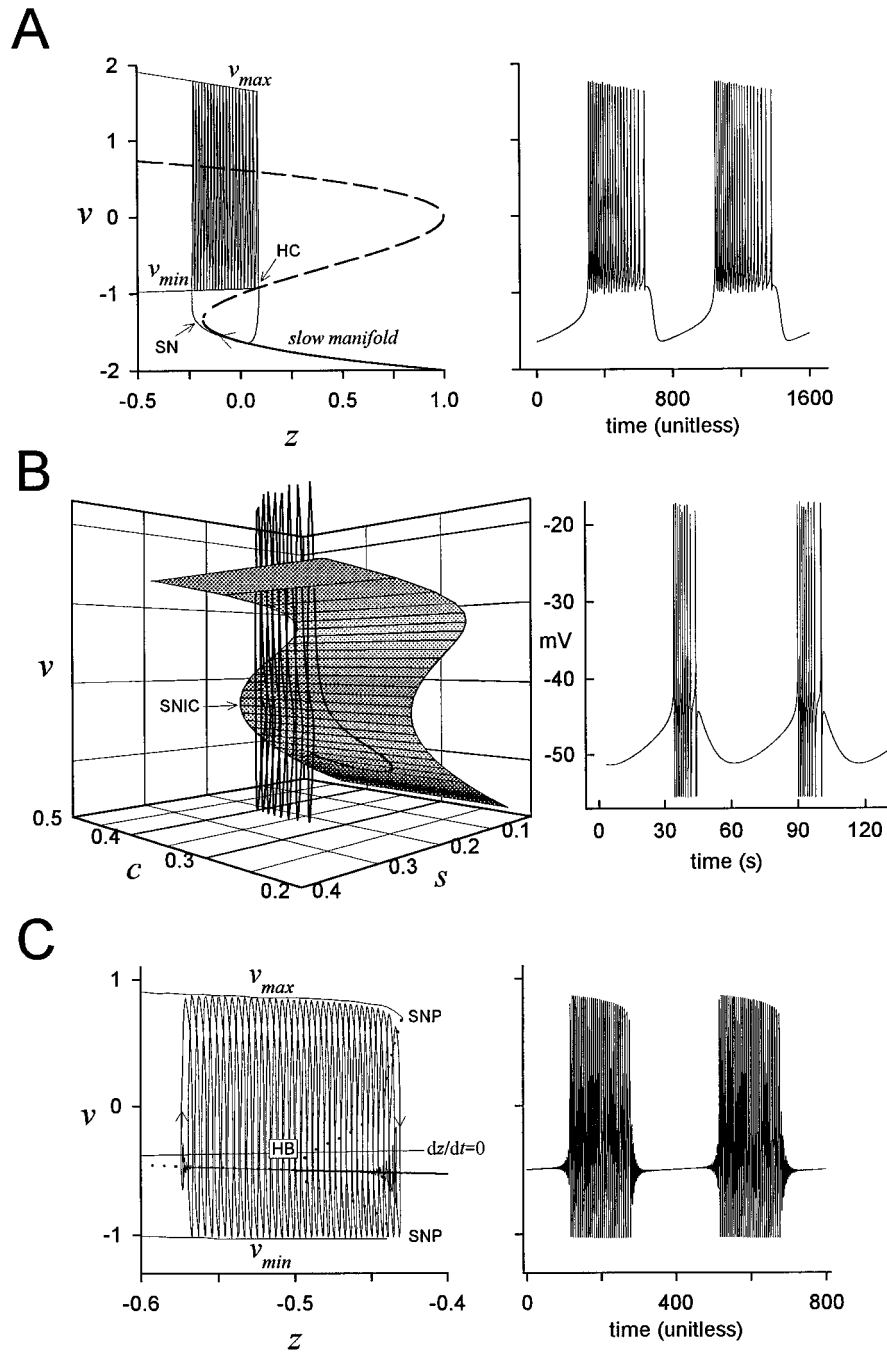
FIGURE 1   Topological and phenomenological features of minimal bursting models. (*A*) The Hindmarsh-Rose model of bistable bursting (Hindmarsh and Rose, 1984; Wang, 1993a). The Z-shaped slow manifold is illustrated in (z, v) state space (*left*). The lower branch of the slow manifold (*solid lines*) contains all stable steady-state solutions to FAST (v_{ss}) and connects to the unstable middle branch of saddle points (*broken lines*) at the left knee of the slow manifold. The upper branch (unstable foci) connects with the middle branch at $z = 1$. The upper branch is surrounded by stable periodic solutions of FAST (v_{osc}) representing action potentials (maximum and minimum voltages of v_{osc} are shown by v_{max} and v_{min}, respectively). The bursting trajectory obtained numerically (*thin solid line*) travels clockwise along the slow manifold (*arrowhead indicating direction is shown on lower stable branch*). The saddle node (SN) and homoclinic bifurcations (HC) associated with burst initiation and termination, respectively, are illustrated. A time series of bursting in the Hindmarsh-Rose model is shown (*right*, same voltage scale as state-space graph on the *left*). (*B*) Parabolic bursting in the Chay-Cook model (Bertram et al., 1995; Chay and Cook, 1988). The slow manifold (*left*) is a Z-shaped surface with identical stable and unstable branches, as in *A*. A bursting trajectory obtained numerically (superimposed) moves clockwise in (s, v, c) space (s plotted in reverse order). The saddle-nodes-on-invariant-circles (SNIC) bifurcations associated with phase transition (Bertram et al., 1995; Guckenheimer et al., 1997; Rinzel and Ermentrout, 1989) (see text) are located at the left knee of the slow manifold, and all share the same s value. A time series of parabolic bursting is shown (*right*). (*C*) The Fitzhugh-Rinzel model of type 3 bursting. We adjusted the parameters to obtain a quiescent phase that settles into its steady-state voltage (compare to figure 4 *A* in Rinzel, 1987). The slow manifold, illustrated in (z, v) space (*left*), is approximately linear (*thick solid line*). At $z = -0.5$, the stable branch containing v_{ss} (center) destabilizes via subcritical Hopf bifurcation (where the eigenvalues of the Jacobian matrix of FAST are: $a \pm bi$ and $a = 0, b \neq 0$) and is surrounded by a stable attracting limit cycle (v_{osc}, shown by maximum and minimum voltages excursions, v_{max} and v_{min}, respectively). The stable branch of limit cycles intersects the branch of unstable limit cycles (*broken lines*) at $z \approx -0.43$, a saddle-node-of-periodics (labeled SNP in the figure) bifurcation associated with burst termination. The dz/dt nullcline is also illustrated (see text for explanation). A bursting trajectory obtained numerically is shown in state space (*left, thin solid lines with arrowheads* indicating direction) and as a time series (*right*).

Traditional bursting neurons share the characteristics derived from a Z-shaped slow manifold, including saddle-node and homoclinic bifurcations mediating phase transition. We classify trigeminal neurons as *traditional* if they exhibit the phenomenological features associated with this topology, but we do not distinguish whether the bursting behavior is bistable or parabolic.

Type 3 bursting does not employ a Z-shaped slow manifold. Instead, the slow manifold is an approximately linear branch of stable foci that destabilize at a subcritical Hopf bifurcation. To initiate the active phase in the Fitzhugh-Rinzel model of type 3 bursting (Appendix), the SLOW subsystem causes a slow passage through the Hopf point. This transition occurs because the system, in its quiescent phase, lies below the dz/dt nullcline (Fig. 1 *C*). In the region of state space below the dz/dt nullcline, $dz/dt < 0$; consequently, z is decreasing and the system moves through the Hopf point. The system tracks the branch of unstable foci (whose vectors are minimal in the vicinity of the bifurcation) after passing the Hopf point, and later spins away from the unstable branch to join the outer stable limit cycle attractor (Fig. 1 *C*). Phenomenologically this results in subthreshold oscillations that grow to full-amplitude spikes after a delay (Baer et al., 1989).

The subcritical Hopf bifurcation of the type 3 model allows stable point and stable oscillatory attractors to coexist near the Hopf point (Rinzel, 1987; Rinzel and Ermentrout, 1989) (Fig. 1 *C, left*, where $-0.5 < z < -0.43$). Therefore, during the active phase when SLOW moves the oscillatory solution back through the Hopf point (z is increasing beyond -0.5; Fig. 1 *C*), the system continues in its

periodic attractor. The system spends time both above and below the dz/dt nullcline during limit cycles in the active phase, the portion for which $dz/dt > 0$ predominates during each spike, causing a net increase in z. Because there is a net increase in z during each spike, z increases throughout the active phase. The spike oscillation ultimately terminates at a saddle-node-of-periodics bifurcation, where the stable oscillatory branch merges with the inner unstable branch of limit cycles associated with the subcritical Hopf structure. The intersection of stable and unstable oscillations annihilates both periodic solutions, causing the system to return to the approximately linear, stable branch of the slow manifold. The cycle restarts as z begins to decrease again (because the system lies below the dz/dt nullcline) (Fig. 1 *C*).

I-V curves and the shape of the slow manifold

The Z-shaped slow manifold required for traditional bursting reflects, in the context of a bifurcation diagram, the presence of NSR in the steady-state *I-V* relationship. In contrast, to produce the flat manifold characteristic of type 3 bursting, a region of NSR in the steady-state *I-V* relationship is not necessary. Therefore, by observing the steady-state *I-V* curve in bursting neurons, we glimpse the topological structure of their slow manifold.

A region of NSR was observed in the steady-state *I-V* relationship of TMNs that burst in the presence of serotonin (Hsiao et al., 1998) (Fig. 2 *A*). Conversely, TIs never exhibited a region of NSR, regardless of protocols used to generate the *I-V* relationship (Fig. 2 *B*). The *I-V* curve of a
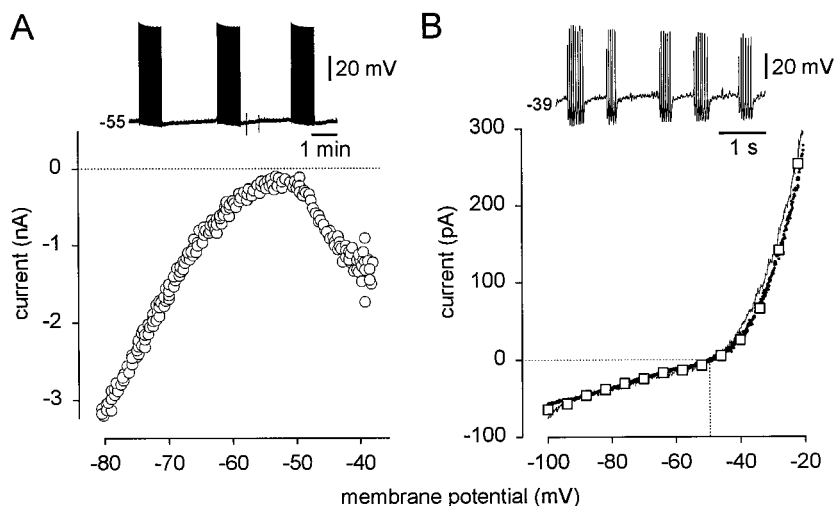

FIGURE 2   The steady-state current-voltage relationship of trigeminal neurons. (*A*) the steady-state *I-V* curve of a TMN in the presence of 10 μM serotonin obtained by a slow voltage ramp protocol (7.5 mV/s). Regenerative inward currents underlying the region of NSR activate at -52 mV. The curve is obscured at potentials more positive than -40 mV due to spike oscillations in unclamped regions of the soma-dendritic membrane. More complete steady-state *I-V* curves for TMNs, obtained in the presence of 10 μM serotonin and 0.5 μM tetrodotoxin, are available (Hsiao et al., 1998). Bursts initiated autonomously in this TMN, because the region of NSR was located in the region of net inward current (*below the zero current axis, dotted line*). Bursting in this TMN is shown in the inset (+0.1 nA holding current). (*B*) Steady-state *I-V* curve in a TI in the presence of 20 μM bicuculline and 5 μM strychnine to block spontaneous inhibitory synaptic noise. Three protocols were used: long-duration voltage step commands (5 s, *open squares*), slow voltage ramps (10 mV/s, *solid line*), and fast voltage ramps (in the presence of 0.5 μM tetrodotoxin to block Na$^+$ spikes) (100 mV/s, *dots*). The inset shows bursting in this TI (+65 pA holding current) (same cell as in Fig. 3).

representative TI was obtained in response to long-duration voltage step commands (5 s), a slow voltage ramp (10 mV/s), and a fast voltage ramp (100 mV/s). The fast ramp protocol was performed in the presence of tetrodotoxin. Slow and fast ramps were used to assess the quasi-steady-state *I-V* relationship, because in some traditional bursting neurons the currents underlying the region of NSR can undergo inactivation (Benson and Adams, 1989; Canavier et al., 1991). These data demonstrate that TMNs, which exhibit a region of NSR, can possess a Z-shaped slow manifold, whereas TIs cannot.

Behaviors in response to current bias

The region of NSR expressed by traditional bursting neurons implies that a stable steady state and a stable oscillatory state can exist, separated by tens of millivolts, on either side of a spike threshold. These states in the *I-V* curve correspond directly to the lower (quiescent) and the upper (oscillatory) branches of the slow manifold. The system can reside at either state, depending on the position of the NSR with respect to the zero-current axis. During bursting, SLOW causes the system to alternate between states. However, the position of the NSR can also be experimentally manipulated by constant current injection. Therefore, if TMNs experience traditional bursting dynamics, then current bias of sufficient magnitude and polarity should lock the neurons into nonalternating quiescent or tonic spiking

behaviors. A representative example of bursting in a TMN is shown in Fig. 3 *A* (*middle trace*). When this cell was biased by hyperpolarizing current injection, it remained quiescent (Fig. 3 *A, bottom trace*). Conversely, when biased with depolarizing current, the cell became tonically active (Fig. 3 *A, top trace*).

We expect type 3 bursting to differ from traditional bursting in several ways. First, type 3 cells should be able to maintain quiescence at more depolarized potentials than in traditional bursting neurons. This is predicted because the negative slope region of the *I-V* curve in traditional bursting creates a range of potentials that are inaccessible to the cell under current-clamp conditions. The neuron is forced to assume either the hyperpolarized (quiescent) or depolarized (oscillatory) state, depending on the position of the NSR with respect to the zero-current axis. Therefore, the traditional burster can only be locked in the quiescent state at subthreshold potentials more negative than the *I-V* curve's turning point (where the NSR begins, e.g., −52 mV in Fig. 2 *A*). Because the type 3 bursting system does not possess NSR, it does not destabilize at subthreshold potentials and can remain quiescent until membrane potential exceeds spike threshold.

However, we must consider the effect of noise in the experimental setting, and the fact that the unstable limit cycle born at the Hopf point acts as a separatrix. As the cell is biased toward spike threshold, the basin of attraction for the stable focus point becomes smaller as the branch of

FIGURE 3   The behavior of trigeminal neurons in response to current bias and trajectories of burst initiation. (*A*) 10 µM serotonin-induced bursting in this TMN (*middle trace*, −0.2 nA holding current) could be converted to stable quiescent behavior (at −70 mV) by increasing the hyperpolarizing current injection to −0.8 nA (*lower trace*), or to tonic spiking activity by sufficient depolarizing current injection (+0.1 nA, *upper trace*). (*B*) An example of burst initiation in TMNs expanded from *A* (*box*). Note the rapid upswing in voltage trajectory. (*C*) Bursting activity in TIs emerged as the cells were progressively depolarized to potentials near and above spike threshold (−45 mV). This TI's resting potential was −65 mV (not shown). At the quiescent potentials −50 and −47 mV, the bias current was +20 and +25 pA, respectively (*lower traces*). These quiescent states were more depolarized than quiescent potentials in TMNs: −47 (*C*) versus −70 mV (*A*). Intermittent discharge occurred near threshold; bias currents were +30 and +45 pA at near-threshold potentials −45 and −43 mV, respectively (*middle traces*). Bursting occurred when TIs were biased to suprathreshold potentials (−39 mV, +65 pA holding current, *top trace*). This TI was recorded in the presence of 20 µM bicuculline and 5 µM strychnine to block spontaneous inhibitory synaptic noise. (*D*) An example of burst initiation in TIs expanded from *C* (*box*). Note the linear voltage trajectory and growing subthreshold oscillations. Voltage calibration applies to all traces. Time calibrations are separate for *A* and *C*.
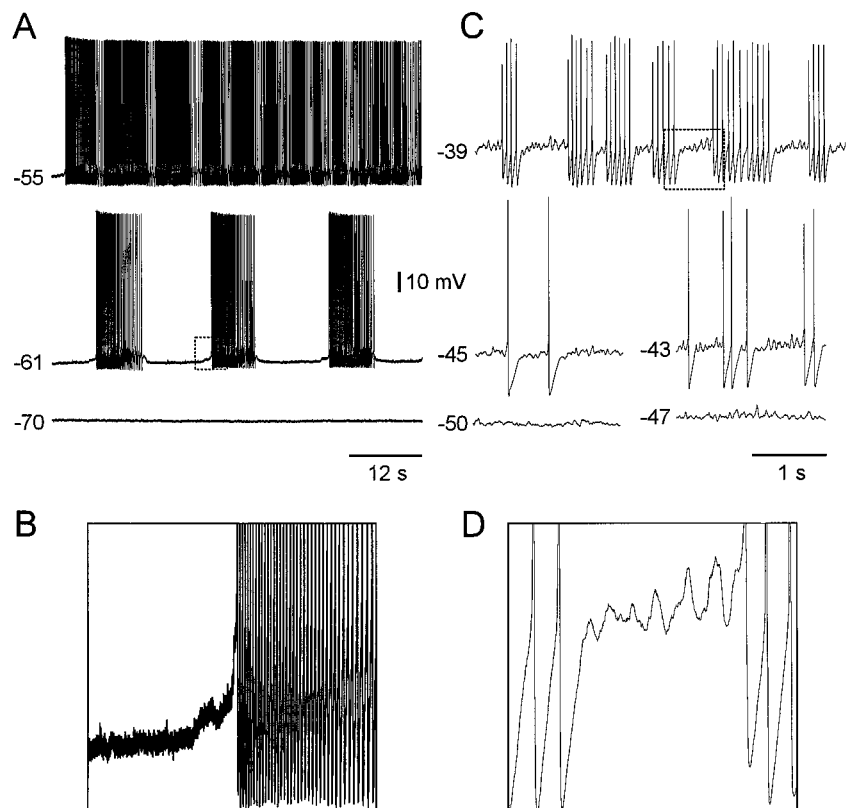
unstable limit cycles converges to the Hopf point (Fig. 1 *C, left*). Consequently, near spike threshold any noise source could cause the system to cross the separatrix and produce spikes. Therefore we predict that type 3 bursting, in an experimental setting (where noise is a factor), should evolve from intermittent spike discharge as the cell is depolarized progressively toward threshold.

TIs satisfy these criteria. The cells are quiescent at rest (−65 mV for the cell in Fig. 3 *C*, not shown), and remain quiescent at more depolarized potentials than TMNs (compare the bottom rows of Fig. 3, *A* and *C*). TIs discharged intermittently when biased near threshold (approximately −45 mV). Intermittent discharge increased with greater depolarization (Fig. 3 *C, middle row*), suggesting sensitivity to intrinsic and synaptic noise. When biased to suprathreshold potentials (−39 mV), bursting resulted (Fig. 3 *C*).

Burst initiation

The membrane potential trajectory in traditional bursting is slow during quiescent phases, governed by the slow membrane processes. However, progressing from the quiescent to the active phase, the cell reaches the membrane potential for activation of inward currents constituting the NSR (Fig. 2 *A*). The regenerative nature of the currents ensures that spike threshold is crossed in a rapid voltage upswing, which tracks the curvature of the slow manifold at its left knee and underlies the prediction that spikes emerge at full amplitude. TMN bursting, expanded near active phase initiation, illustrates this characteristic transition (Fig. 3 *B*).

In contrast, the active phase of type 3 bursting initiates at a Hopf bifurcation that predicts the emergence of subthreshold oscillations that grow to full-amplitude spikes. Further-

more, the trajectory through a Hopf bifurcation is not expected to illustrate a voltage upswing, because the slow manifold is approximately linear, not Z-shaped. Consistent with this mechanism, TIs approaching the active phase exhibit a linear voltage trajectory accompanied by growing oscillations (maximum amplitude 10 mV) preceding full-amplitude spikes (Figs. 3 *D* and Fig. 4 *B*).

Burst termination

In traditional bursting neurons, the active phase terminates via homoclinic orbits. Phenomenologically, this produces a monotonic spike frequency decline near burst termination. To examine the spike frequency profile of TMNs during bursting, the intraburst instantaneous spike frequency was plotted below burst episodes in time series (Fig. 4 *A*). Frequency was highest near active phase initiation and exhibited a quasimonotonic decay approaching termination.

A similar analysis of intraburst spike frequency in TIs illustrates nearly constant spike frequency throughout the burst episodes (Fig. 4 *B*). When declining spike frequency is not present as burst termination is approached, a homoclinic mechanism is impossible. The alternative for burst termination is the saddle-node-of-periodics bifurcation for which intraburst spike frequency is indeterminate (Bertram et al., 1995), though bounded (Guckenheimer et al., 1997; Rinzel and Ermentrout, 1989). This mechanism is consistent with the spike frequency profile of TIs.

DISCUSSION

We identify the mechanism of bursting in trigeminal neurons based on phenomenological predictions of minimal
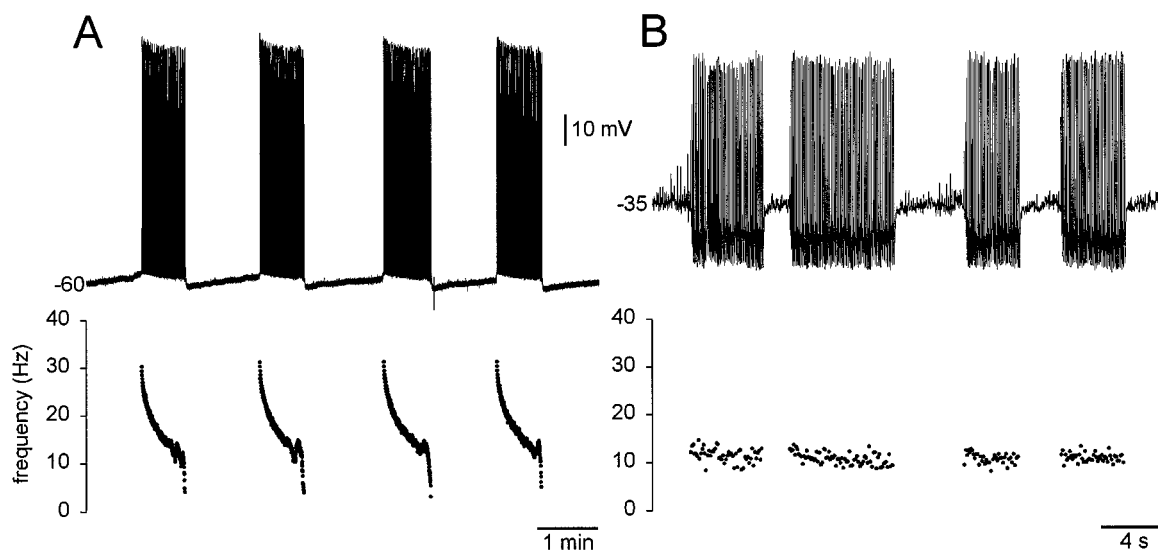

FIGURE 4   The phenomenology of burst termination in trigeminal neurons. (*A* and *B*) Bursting behavior is illustrated for a TMN (*A*) and a TI (*B*). The instantaneous spike frequency was plotted synchronously (*lower*) with the same ordinate axis for frequency (Hz) in *A* and *B*. Voltage calibration applies to *A* and *B*; time calibrations are separate. Holding currents in *A* and *B* were 0 nA and +18 pA, respectively. Records from the TMN in *A* were obtained in the presence of 10 μM serotonin. Records from the TI in *B* were obtained in the presence of 20 μM bicuculline, 5 μM strychnine, 10 μM 6-cyano-7-nitroquinoxaline-2,3-dione disodium (CNQX), and 10 μM *d,l*-2-amino-5-phosphonovaleric acid (APV) to block all spontaneous synaptic activity in this cell.

models. These features include voltage trajectory, intraburst spike frequency profile, and qualitative response to current bias, which is behavior related to the topology of the slow manifold.

Traditional mechanism in TMNs

Burst initiation in TMNs occurs via saddle-node bifurcation. The region of NSR in TMNs activates near -52 mV (Fig. 2 A) (Hsiao et al., 1998). This turning point of the I-V curve is subthreshold and corresponds to the left knee of the Z-shaped slow manifold. The voltage upswing that occurs during burst initiation is consistent with the trajectory predicted by this shape. Because the region of NSR is located in the area of net inward current (i.e., below the zero-current axis; Fig. 2 A), membrane potential approaches this turning point autonomously, albeit slowly.

The decline in spike frequency that precedes burst termination in TMNs suggests an approach to a homoclinic orbit. However, whereas homoclinic mechanisms of termination require spike frequency decay, the spike frequency profile for burst termination through a saddle-node-of-periodics is indeterminate, though bounded. Theoretically, bursts may initiate at a saddle-node bifurcation, yet terminate in a saddle node of periodics (Bertram et al., 1995). Therefore, the possibility that TMN bursts terminate in a saddle node of periodics cannot be eliminated. Nevertheless, we favor the homoclinic mechanism for TMNs. First, the saddle-node to saddle-node-of-periodics variation of bursting identified by Bertram et al. (1995) was confined to a relatively small region of parameter space. Second, the saddle-node-of-periodics bifurcation in nerve models is usually connected to a subcritical Hopf bifurcation by the branch of unstable limit cycles (Fig. 1 C). Therefore, the stable branch of foci, which emerge from the Hopf point and become globally attracting at the saddle-node-of-periodics bifurcation, must be located between the maximum and minimum voltage amplitudes of the stable limit cycle (see Fig. 1 C, left). TMNs often hyperpolarize at burst termination to levels more negative than the minimum voltage of the action potential (e.g., Fig. 4 A); this is inconsistent with the topology of a saddle node of periodics and favors a homoclinic mechanism such as that in Fig. 1 A.

The responses of TMNs to current bias further support the presence of a Z-shaped slow manifold, as suggested by the I-V curve. TMNs were locked into silent or tonic spiking behaviors when biased away from their "normal" bursting state by hyper- or depolarizing current injection (Fig. 3 A). Topologically, maintained quiescence corresponds to confining the system to the lower stable branch of the slow manifold (to the right of the left knee). Conversely, tonic spiking corresponds to the system confined to the upper oscillatory branch of the slow manifold (left of the left knee). The requisite current bias must be of sufficient magnitude to override the tendency of the SLOW subsystem to induce phase alternation by causing the system to cross the left knee of the slow manifold.

A novel bursting mechanism in TIs

Burst initiation in TIs must occur via Hopf bifurcation, because these neurons lack the region of NSR required for a saddle-node bifurcation and exhibit a linear voltage trajectory accompanied by growing subthreshold oscillations at burst onset. Hopf bifurcations in excitable membrane models are generally subcritical (Fitzhugh, 1961; Rinzel and Ermentrout, 1989). Because a subcritical Hopf bifurcation surrounded by a stable limit cycle produces the topological structure for a saddle node of periodics, and TIs exhibit no noticeable decline in spike frequency during the active phase (Fig. 4), burst termination in TIs is best explained by the saddle-node-of-periodics mechanism.

The existence of quiescent phases while membrane potential is biased to suprathreshold levels (e.g., -39 or -35 mV in Figs. 3 and 4, respectively) depends on the mathematics of slow passage through the Hopf bifurcation. When ramped slowly, the excitable system destabilizes after the control parameter exceeds the Hopf point predicted by bifurcation analysis; this is due to a delay effect (Baer et al., 1989). In terms of our observable quantity, voltage, the cell destabilizes only after passing threshold (as determined by rheobasic step commands).

The bursting activity in neonatal rat TIs represents the first documented example of Bertram's (1995) type 3 bursting in a biological system. Although a type 3 mechanism has been proposed (Wang, 1993b) for 10–50-Hz neuronal oscillations occurring in guinea pig cortex (Llinás et al., 1991) and rat thalamus (Pinault and Deschenes, 1992), the original experimental studies characterized the oscillations without investigating the underlying dynamics from a topological perspective. Furthermore, a recent report illustrates such 30–40-Hz oscillations, whose phenomenology is equally consistent with a traditional bursting mechanism (Steriade et al., 1998). Therefore, the TI is the first bona fide example of type 3 bursting.

Physiological implications

Type 3 bursting behavior is sensitive to intrinsic and synaptic noise. Perturbations during the quiescent phase can cause sporadic action potentials or prematurely initiate an abbreviated active phase by causing the system to cross the separatrix created by the branch of unstable limit cycles born at the subcritical Hopf bifurcation. Because the separatrix converges at the Hopf point, effective perturbations can be of extremely small amplitude in the vicinity of the bifurcation. This explains why TIs discharged intermittently near threshold (Fig. 3 C). Noise sensitivity causes variability in the frequency and duration of burst cycles and may interrupt the regularity of bursting rhythms. However, this sensitivity to perturbation may also facilitate phasic control of TIs by small-amplitude synaptic inputs in the context of network activity.

In contrast to type 3 bursting systems such as the TI, traditional bursting systems require larger perturbations for

phasic modulation. In bistable bursting (Fig. 1 *A*), the two stable states are separated by tens of millivolts in the *I-V* curve (and reflect separate branches of the slow manifold). Therefore the perturbation required to move the system between basins of attraction is much larger than that required to move a type 3 neuron across its separatrix. Although parabolic bursting systems do not exhibit hysteresis-based bistability (e.g., Fig. 1 *A*), they do exhibit multistability among periodic attractors (Butera, in press; Canavier et al., 1993), and are sensitive to phasic perturbation (Demir et al., 1997). Again, the perturbations required to move between basins of attraction in a parabolic bursting system are relatively large compared to type 3 neurons.

It is believed that the intrinsic autorhythmicity of bursting neurons can contribute to the genesis of rhythmical motor behavior (Marder and Calabrese, 1996). Neural pacemakers are hypothesized to interact with a network to produce final output patterns (for example, see Smith, 1997). Depending on the need for modification of motor patterns, it may be advantageous in some motor systems to incorporate pacemaker neurons with high sensitivity to perturbation of phase. Whereas traditional bursting systems are less sensitive to perturbation (i.e., require large amplitude perturbations), the novel type 3 bursting behavior that we characterize in TIs is profoundly sensitive to small-amplitude phasic perturbation.

APPENDIX

The Hindmarsh-Rose model for bistable bursting, abstracted to arbitrary voltage and time units for analytical simplicity (Hindmarsh and Rose, 1984; Wang, 1993a), is written as follows:

$$\text{FAST:} \quad dv/dt = w - v^3 + 3v^2 - z$$

$$dw/dt = 1 - 5v^2 - w$$

$$\text{SLOW:} \quad dz/dt = \alpha(v - [(z - z_0)/4]),$$

$$\alpha = 0.004 \text{ and } z_0 = 4.$$

The Chay-Cook model for parabolic bursting (Bertram et al., 1995; Chay and Cook, 1988), parameterized in biophysically realistic units, is

$$\text{FAST:} \quad dv/dt = -[I_{Ca}(v, s) + I_K(v, n) + I_L(v)]/C_m$$

$$dn/dt = \lambda(n_\infty(v) - n)/\tau_n(v)$$

$$\text{SLOW:} \quad ds/dt = (s_\infty(v, c) - s)/\tau_s(v, c)$$

$$dc/dt = \alpha[-fI_{Ca}(v, s) - k_c c].$$

All ionic currents are described by chord conductance equations:

$$I_{Ca}(v, s) = I_i(v) + I_s(v, s)$$

$$I_i(v) = g_i m_\infty(v)(v - E_{Ca})$$

$$I_s(v, s) = g_s s(v - E_{Ca})$$

$$I_K(v, n) = g_K n(v - E_K)$$

$$I_L(v) = g_L(v - E_L).$$

Time constants and activation functions are

$$x_\infty(v) = (1 + \exp[(E_x - v)/S_x])^{-1}, \quad (x = m, n)$$

$$s_\infty(v, c) = (1 + \exp[2A(v, c)])^{-1}$$

$$\tau_n(v) = \tau_{n0}(1 + \exp[(v - E_n)/S_n])^{-1}$$

$$\tau_s(v, c) = \tau_{s0}[2 \cosh(A(v, c))]^{-1}, \quad A(v, c)$$

$$= (E_s + S_s \ln(c_0) - v)/(2 S_s),$$

with parameters $c_0 = c/(1 \ \mu M)$, $g_i = 250$ pS, $g_s = 10$ pS, $g_K = 1300$ pS, $g_L = 50$ pS, $\lambda = 0.6$, $\alpha = 0.0015$, $k_c = 0.03$ ms^{-1}, $E_{Ca} = 100$ mV, $E_K = -80$ mV, $E_L = -60$ mV, $C_m = 4524$ fF, $\tau_{n0} = 9.09$ ms, $\tau_{s0} = 10$ s, $E_m = -22$ mV, $E_n = -9$ mV, $E_s = -22$ mV, $S_m = 7.5$ mV, $S_n = 10$ mV, $S_s = 10$ mV, and $f = 5.727 \times 10^{-6} \ \mu M$ fA^{-1} ms^{-1}.

The Fitzhugh-Rinzel model of novel (type 3) bursting (Rinzel, 1987) is also abstracted to arbitrary voltage and time units for analytical simplicity:

$$\text{FAST:} \quad dv/dt = w - 4(v^3 - v) - z$$

$$dw/dt = -(4v + 1 + w)$$

$$\text{SLOW:} \quad dz/dt = \alpha(1.25v - [(z - z_0)/4]),$$

$$\alpha = 0.003 \text{ and } z_0 = 1.33.$$

REFERENCES

Ashcroft, F., and P. Rorsman. 1989. Electrophysiology of the pancreatic β-cell. *Prog. Biophys. Mol. Biol.* 54:87–143.

Atwater, I., C. M. Dawson, A. Scott, G. Eddlestone, and E. Rojas. 1980. The nature of the oscillatory behavior in electrical activity for pancreatic β-cells. *In* Biochemistry Biophysics of the Pancreatic β-Cell. G. Thieme, editor. Springer Verlag, New York. 100–107.

Av-Ron, E., H. Parnas, and L. A. Segel. 1993. A basic biophysical model for bursting neurons. *Biol. Cybern.* 69:87–95.

Baer, S. M., T. Erneux, and J. Rinzel. 1989. The slow passage through a Hopf bifurcation: delay, memory effects, and resonance. *SIAM J. Appl. Math.* 49:55–71.

Benson, J. A., and W. B. Adams. 1989. Ionic mechanisms of endogenous activity in molluscan burster neurons. *In* Neuronal and Cellular Oscillators. J. W. Jacklet, editor. Marcel Dekker, New York. 87–120.

Bertram, R., M. J. Butte, T. Kiemel, and A. Sherman. 1995. Topological and phenomenological classification of bursting oscillations. *Bull. Math. Biol.* 57:413–39.

Butera, R. J. 1998. Multistability in bursting neurons. *Chaos.* (in press).

Butera, R. J., Jr., J. W. Clark, Jr., and J. H. Byrne. 1996. Dissection and reduction of a modeled bursting neuron. *J. Comput. Neurosci.* 3:199–223.

Canavier, C. C., D. A. Baxter, J. W. Clark, and J. H. Byrne. 1993. Nonlinear dynamics in a model neuron provide a novel mechanism for transient synaptic inputs to produce long-term alterations of postsynaptic activity. *J. Neurophysiol.* 69:2252–2257.

Canavier, C. C., J. W. Clark, and J. H. Byrne. 1991. Simulation of the bursting activity of neuron R15 in *Aplysia*: role of ionic currents, calcium balance, and modulatory transmitters. *J. Neurophysiol.* 66:2107–2124.

Chay, T. R., and D. L. Cook. 1988. Endogenous bursting patterns in excitable cells. *Math. Biosci.* 90:139–153.

Demir, S. S., R. J. Butera, Jr., A. A. DeFranceschi, J. W. Clark, Jr., and J. H. Byrne. 1997. Phase sensitivity and entrainment in a modeled bursting neuron. *Biophys. J.* 72:579–594.

Fitzhugh, R. 1961. Impulses and physiological states in models of nerve membrane. *Biophys. J.* 1:445–466.

Guckenheimer, J., R. Harris-Warrick, J. Peck, and A. Willms. 1997. Bifurcation, bursting, and spike frequency adaptation. *J. Comput. Neurosci.* 4:257–277.

Hindmarsh, J. L., and R. M. Rose. 1982. A model of the nerve impulse using two first-order differential equations. *Nature.* 296:162–164.

Hindmarsh, J. L., and R. M. Rose. 1984. A model of neuronal bursting using three coupled first order differential equations. *Proc. R. Soc. Lond. Biol.* 221:87–102.

Honerkamp, J., G. Mutschler, and R. Seitz. 1985. Coupling of a slow and a fast oscillator can generate bursting. *Bull. Math. Biol.* 47:1–21.

Hsiao, C.-F., C. A. Del Negro, P. R. Trueblood, and S. H. Chandler. 1998. The ionic basis for serotonin-induced bistable membrane properties in guinea pig trigeminal motoneurons. *J. Neurophysiol.* (in press).

Li, Y.-X., R. Bertram, and J. Rinzel. 1996. Modeling *N*-methyl-D-aspartate-induced bursting in dopamine neurons. *Neuroscience.* 71: 397–410.

Llinás, R., A. Grace, and Y. Yarom. 1991. In vitro neurons in mammalian cortical layer 4 exhibit intrinsic oscillatory activty in the 10–50-Hz frequency range. *Proc. Natl. Acad. Sci. USA.* 88:897–901.

Marder, E., and R. L. Calabrese. 1996. Principles of rhythmic motor pattern generation. *Physiol. Rev.* 76:687–717.

Pinault, D., and M. Deschenes. 1992. Voltage-dependent 40-Hz oscillations in rat reticular thalamic neurons in vivo. *Neuroscience.* 51: 245–258.

Rinzel, J. 1987. A formal classification of bursting mechanisms in excitable systems. *In* Mathematical Topics in Population Biology, Morpho-genesis and Neurosciences. Lecture Notes in Biomathematics, Vol. 71. E. Teramoto and M. Yamaguti, editors. Springer Verlag, Berlin. 267–281.

Rinzel, J., and G. B. Ermentrout. 1989. Analysis of neural excitability and oscillations. *In* Methods in Neuronal Modeling. C. Koch and I. Segev, editors. MIT Press, Cambridge. 135–169.

Rinzel, J., and Y. S. Lee. 1986. On different mechanisms for membrane potential bursting. *In* Nonlinear Oscillations in Biology and Chemistry. Lecture Notes in Biomathematics, Vol. 66. H. G. Othmer, editor. Springer Verlag, New York. 19–33.

Rinzel, J., and Y. S. Lee. 1987. Dissection of a model for neuronal parabolic bursting. *J. Math. Biol.* 25:653–675.

Schwindt, P. C., and W. E. Crill. 1980. Role of a persistent inward current in motoneuron bursting during spinal seizures. *J. Neurophysiol.* 43: 1700–1724.

Smith, J. C. 1997. Integration of cellular and network mechanisms in mammalian oscillatory motor circuits: insights from the respiratory oscillator. *In* Neurons, Networks, and Motor Behavior. P. S. G. Stein, S. Grillner, A. I. Selverston, and D. G. Stuart, editors. MIT Press, Cambridge. 97–104.

Smith, T. G. 1975. Requirements for bursting pacemaker potential activity in molluscan neurones. *Nature.* 253:450–452.

Steriade, M., I. Timofeev, N. Durmuller, and F. Grenier. 1998. Dynamic properties of cortico-thalamic neurons and local cortical interneurons generating fast rhythmic (30–40 Hz) spike bursts. *J. Neurophysiol.* 79:483–490.

Wang, X.-J. 1993a. Genesis of bursting oscillations in the Hindmarsh-Rose model and homoclinicity to a chaotic saddle. *Physica D.* 62:263–274.

Wang, X. J. 1993b. Ionic basis for intrinsic 40 Hz neuronal oscillations. *Neuroreport.* 5:221–224.